Processing and Characterization of Hierarchical Surface Coatings for Titanium Implants

Prepared By:
Courtney Alison Gegg

Faculty Advisors:
Dr. Michael K. West
REU Site Director, Department Head of Materials and Metallurgical Engineering

Dr. Grant A. Crawford
Assistant Professor, Department of Materials and Metallurgical Engineering

Dr. Alfred R. Boysen
Professor, Department of Humanities

Table of Contents

Abstract

Osteoarthritis, a disease that currently affects 27 million Americans, is the most common cause of physical disability in the United States. The disease involves the degradation of joints in the body, including the cartilage surrounding the joints, as well as the bone underlying the affected cartilage. Pain, limited movement, and stiffness in the effected joint is common. To treat this disease, surgical procedures, such as replacement surgeries, are performed. Titanium and titanium alloys are commonly used in load bearing implants (e.g. knee and hip) due to their excellent strength-to-weight ratio and corrosion resistance.

This study investigates the processing, microstructure characterization and biological response of hierarchical surface modifications on titanium substrates. Hierarchical surface modifications consisting of grid-like structures on the microscale and TiO_2 nanotubes were fabricated using laser powder deposition in conjunction with anodic oxidation. Furthermore, this study evaluated the effectiveness of wirebrush cleaning to improve the function of the micro-scale features. As processed, surface modifications were characterized using optical microscopy, scanning electron microscopy, surface wettability characterized by contact angle, and in vitro biological response of mouse pre-osteoblasts characterized by fluorescence intensity.

Titanium substrates with nano-scale surface features showed lower contact angles and fostered greater cell attachment. Titanium substrates with micro-scale surface features that were void of any contamination and cleaned of possibly disadvantageous particles also showed lower contact angles and had greater cell adhesion.

These results suggest that the hierarchical coating, as well as cleaning of the as-processed micro-scale surface features, can beneficially increase the biological properties of the titanium substrates. Optimization of micro-scale feature size will further elucidate the benefits of the making the hierarchical surface coating better suited for clinical use.

Broader Impact

Osteoarthritis, a disease characterized by the degradation of articular cartilage as well as bone underlying the cartilage, is the most common form of arthritis [5, 12]. Currently, osteoarthritis affects 27 million American, which is over 12% of the adult population. It is estimated to cost Americans $89.1 billion annually [3, 4].

Many treatments are available for osteoarthritis; however, symptom relief is the aim of all treatments as there is currently no cure for osteoarthritis. Most commonly, treatments such as weight reduction, exercise, and assistive devices (braces, walking canes, etc.) are used first. Additionally, pharmacologic therapies, such as non-steroidal anti-inflammatory drugs (NSAIDs) and painkillers can be employed [9]. Due to their invasive nature, surgical treatments are usually considered only when previous treatments have failed [9]. Nevertheless, a significant number of surgical procedures to treat osteoarthritis are performed. In the U.S. alone, more than 285,000 total hip replacements and 600,000 knee replacements are completed each year [1, 2].

Quite often, titanium is used as the implant biomaterial to replace hard tissues in the body that are damaged due to normal wear and tear, trauma, or aging. Titanium is a choice biomaterial due to its good mechanical properties, corrosion resistance, high strength-to-weight ratio, and perhaps most importantly, it's excellent biocompatibility [8].

Introduction

Although titanium is widely used today to replace tissues, long-term clinical success is hindered by the limited osseointegration of titanium. When titanium is

implanted in the body, the bone and implant are only partially integrated, often causing the implant to become loosened from the bone. Because of this, it has been the focus of scientists to modify the surface of titanium metal to create stronger mechanical fixation between the bone and implant. Recent studies have shown micro-scale roughness on the biomaterial surface increases interlocking between implant and bone [6, 11]. Additionally, nano-scale surface structures increase osteoblast (bone-forming cell) function [7, 14, 15]. It is hypothesized that combining both micro- and nano- scale surface features into a single hierarchical coating can further improve osseointegration, and as a result, implant success.

The motivation behind this study lies behind data collected by Ellen Sauter, a previous master's student in the Materials Engineering and Science Program at SDSM&T. Sauter created a hierarchical coating on titanium by using laser powder deposition to create a surface grid on the micro-scale, and anodic oxidation to create surface nano-scale tubes, directly superficial to the microgrid. Sauter's study employed four experimental groups:

1. Flat (no microgrid) without nanotubes

2. Flat (no microgrid) with nanotubes

3. Microgrid without nanotubes

4. Microgrid with nanotubes

She then assessed the biological performance of her samples by culturing cells, seeding them on the samples, and four days later, measuring cell viability (measured as the amount of living cells in a given area). Figure 1 shows the cell density for various surface treatments employed in Sauter's Master's thesis [13].
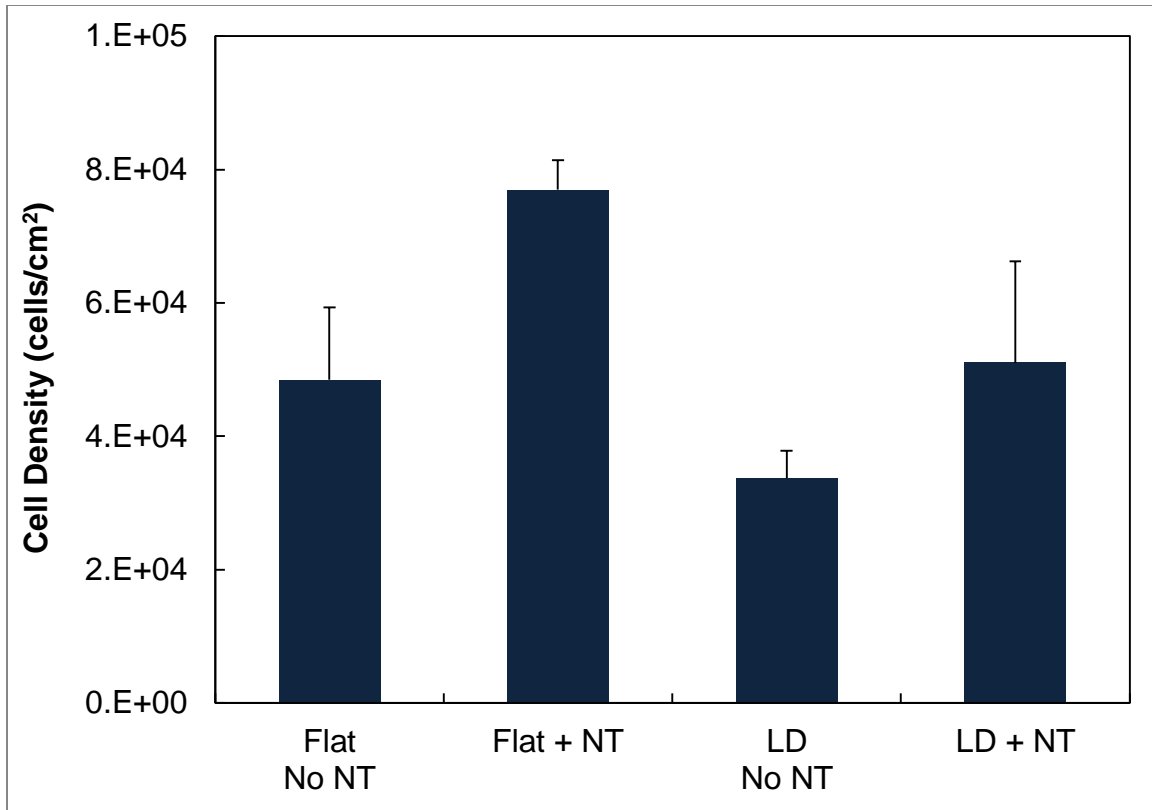
Figure 1. Previous cell density data from Sauter's Master's Thesis.

From inspection of Figure 1, samples with surface nanotubes showed higher cell density, a sign of increased osteoblast function. However, samples with surface microgrids yielded lower cell density data when compared to samples that had no micro-scale features on their surfaces, a very unexpected result.

The goal of this project was to identify what caused the discrepancy between Sauter's experimental results and the expected results, which are based on literature. The two preliminary hypotheses for this were:

1)   Unmelted laser deposition powder particles remained on the surface of the microgrided samples, therefore blocking cells from attaching.

2)   A thick layer of titanium dioxide, formed due to poor atmosphere control during deposition, obstructed the cells from attaching to the titanium.

As is evident, both preliminary explanations for the discrepancy center on the laser deposition (LD) process; because of this, the goal of this project was to improve the processing of the surface microgrid. To address the unmelted LD powder, a wire brush was used on the samples after LD to try and eliminate the grid of the particles. To lessen the aluminum oxide layer, the microgrid itself will be shrunk to fit within the titanium substrate boundaries. Many of Sauter's substrates had microgrids that had been deposited on the entire substrate, as well as over the sides. This means that the laser being used to deposit possibly welded the samples to the aluminum mount they were on, perhaps leading to aluminum sputtering.

By removing unmelted LD particles and the aluminum oxide on titanium surfaces, the substrate properties are hypothesized to improve, and with that, biological performance.

Procedure

1. Titanium Substrates

This study employed 99.7% pure titanium sheets, 2.0mm thick (Sigma-Aldrich). To begin the study, samples measuring 1.2 cm x 1.2 cm x 2.0 mm were cut from a sheet, using a precision saw.

2. Polishing

After cutting samples to the correct dimensions, the samples were polished on a grinder-polisher using silicon carbide paper (Leco). Polishing with 400, 600, 800, and

1200 grit paper, in that respective order, was followed by a final ten-minute polishing on felt paper with 1μm alumina. Following this, three surface roughness measurements for each sample were taken and averaged. Samples were polished to an average roughness of 0.1261 μm ± 0.026 μm.

3. Laser Powder Deposition

Microgrids were laser powder deposited on the surface of the polished titanium substrates using a Micro Laser Additive Manufacturing VDK 3000 LASER Deposition System, conducted under an argon atmosphere, purged of oxygen. The powder used was gas atomized powder, commercially pure, grade 1, titanium powder with a mesh size of -120 +200. Samples were deposited with a laser power of 120 W and a travel speed of 10 mm/s. After deposition, each sample was sonicated in deionized water for five minutes for cleansing and holes (1/16" diameter) were drilled upper center in all samples.

3.1 Microgrid Characterization

After laser deposition, the as deposited grids were characterized to measure grid dimensions using a field emission scanning electron microscope (FE-SEM). Grid pore size was measured as shown in Figure 2:
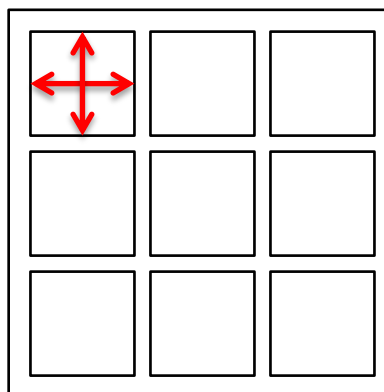

Figure 2. Top-down view of microgrid. Red arrows indicate directions in which pore size was measured.

4. Wire Brush

Samples chosen to receive wirebrush treatment underwent one minute of rigorous brushing, followed by two minutes of sonication in deionized water. This process was repeated twice, for a total of two minutes of brushing and four minutes of sonication per sample. Images with a scanning electron microscope were taken before and after wirebrush treatment to determine the ability of the wirebrush to remove the particles.

5. Anodic Oxidation

Using a double electrode, electrolytic cell, nanotubes were created on the surface of the microgrided samples. The creation of the nanotubes is a result of two competing processes: the growth of titanium oxide (equation 1), followed by the localized dissolution of titanium oxide (equation 2).

$$Ti + O_2 \rightarrow TiO_2 \qquad\qquad\qquad (1)$$

$$TiO_2 + 6F^- + 4H^+ \rightarrow TiF_6^{2-} + 2H_2O \qquad\qquad (2)$$
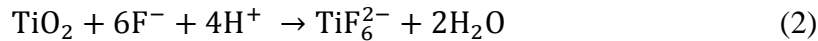
In this electric circuit, the titanium sample acts as the anode (positive terminal), and a platinum-covered mesh acts as the cathode (positive terminal). Prior to oxidation, the anode and cathode were cleaned by sonication for five minutes. The anode and cathode were then taped in placed on opposite sides of a 250 mL plastic beaker.

The electrolyte solution consisted of 0.1 M NaF, 0.2 M $C_6H_8O_7$, and 1 M H_2SO_4 in deionized water. After making the electrolyte solution, the pH was set to 4.0 by the addition of NaOH. The completed electrolyte solution was then poured into a 250 mL plastic beaker containing the electrodes. The cathode was directly connected to the negative lead of the power supply and the anode was connected to the positive lead, by

use of a titanium wire. The anodization process was conducted at a constant 20 V of DC power for 6 hours.

5.1 Nanotube Characterization

After anodic oxidation, the nanotubes created were characterized to measure nanotube dimensions using a field emission scanning electron microscope (FE-SEM). Nanotube lengths and diameters were measured as shown in Figure 3 and 4, respectively. Ten measurements of length of ten different nanotubes were taken, and then averaged for the nanotube length reported. Ten measurements of diameter of five different nanotubes were taken: five measurements in one direction and five measurements in a direction perpendicular to the original direction. These ten measurements were then averaged to obtain the nanotube diameter reported.
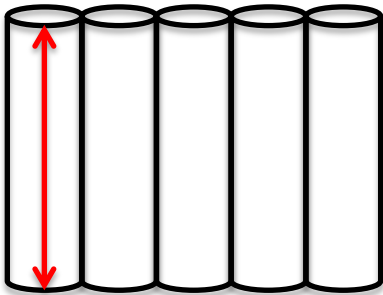

Figure 3. Side-view of nanotubes. Red arrow indicates way in which nanotube length was measured.
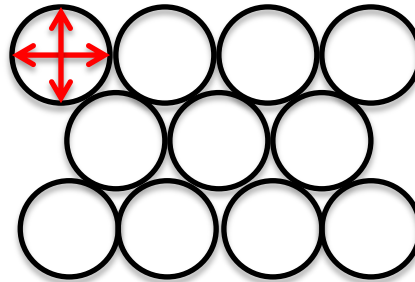
Figure 4. Top-down view of nanotubes. Red arrows indicate way in which nanotube diameter was measured.

6. Contact Angle

Contact angle is a measure of the wettability of a surface. The sessile drop method was used in this study to measure contact angle. In this method, a syringe was used to place a drop (5 μL) of deionized water onto each sample, and the contact angle was measured using DROPimage Advanced software as shown in the schematic depicted

11

in Figure 5. Three different locations on each sample were used to calculate contact angle. For each individual measurement, a left and a right contact angle were measured which must be within six degrees of each other to be considered valid. The six different measurements were then averaged to get a representative contact angle for each sample.
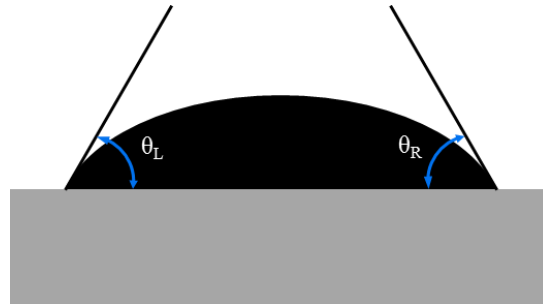

Figure 5 [13]. Schematic of contact angle measurements. Three different locations on each sample were measured, each measurement consisting of a left and right contact angle. The six measurements were then averaged.

7. Biological Assessment

7.1 Cell Culture

Mouse pre-osteoblasts (MC3T3-E1 subclone 4, ATCC® CRL-2593™, Manassas, VA) were cultured in HyClone MEM Alpha Modification 1X (Thermo Scientific) media, supplemented with 10% bovine serum albumin and 1% penicillin-streptomycin. Culture media was exchanged every two days during culture. After 10 days of culture, the cells were removed from the culture flask by trypsinization by the addition of 1% trypsin-EDTA to the flask, which was promptly incubated for two minutes after the trypsin addition. The loose cells were then suspended in culture media, centrifuged, separated from the supernatant, and then resuspended in 10 mL of culture media. Cells were then counted using a hemocytometer. Samples were sonicated in acetone, rinsed with deionized water, and then autoclaved at $250^{\circ}C$ for 30 minutes prior to biological testing.

7.2 Cell Morphology

To study the morphology, $1x10^5$ cells were plated on one sample. Previous work by Sauter had shown little morphologic differences amongst substrate groups, so for this morphology study, only one sample was used, strictly for determining cells in this study were roughly equivalent to the cells used in Sauter's study. A laser deposited microgrid sample was used for morphology. After placing the set amount of cells onto the sample, the sample was incubated for five minutes before adding an additional 5 mL of culture media to the sample, and replacing in the incubator. After four hours, the sample was removed from the incubator, washed with PBS, and fixed with 2.5% glutaraldehyde in 100mM cocodylate buffer pH 7.2 by incubation upon ice for one hour. The sample was then washed with additional 100mM cocodylate buffer pH 7.2, followed by a wash with deionized water. The sample was then dehydrated in ascending ethanol percentage solutions (50, 60, 70, 80, 90, 100, respectively) for 15 minutes each. After dehydration, the sample was air dried and imaged on the scanning electron microscope.

7.3 Cell Viability

To assess the biological response to the substrates, $1x10^5$ cells were plated on each sample. After placing the set amount of cells onto the sample, the samples were incubated for five minutes before adding an additional 5 mL of culture media to each sample, and replacing in the incubator. After two days of incubation, culture media was exchanged. After four days of incubation, the samples were removed from the incubator, washed with PBS, fixed in a 1.5% formaldehyde solution in PBS, and then permeabilized with cold methanol for 20 minutes. Samples were then rinsed of the methanol and dyed with Hoechst 33258 dye at a concentration of 2uL dye/10mL PBS, which selectively

stained the nuclei of live cells. After 15 minutes of staining with dye, the samples were

rinsed with PBS. The samples were then imaged with a fluorescent microscope (VSC

6000). All images were taken with the exact same conditions. Due to the extreme

amount of cell attachment to the substrates, traditional cell counting as a way of

quantifying the data was rendered unmanageable. Instead, two pictures of each substrate,

for a total of 16 images, were changed into 8-bit gray scale pictures using an image

analysis program (ImageJ). The mean gray scale value was then calculated, which is a

representation of fluorescence intensity. Using the traditional RGB color model, a value

of 0 represents black and a value of 255 represents white. Therefore, with the gray scale

fluorescent images, the live nuclei stain brightest, and as a result, take on the RBG value

of 255. Black spaces on the substrate, which have no cells attached to them, take on the

RBG value of 0.

Study Design

This study employed four different groups, each group with a sample number of

n=2, for a total of 8 samples. All groups had a microgrid deposited onto their surfaces.

Half of the groups (2) then received wirebrush treatment, and the other half did not.

Within the groups of 2, one of the groups then underwent anodic oxidation to form

nanotubes on its surface. This layout allowed the researcher to determine how the factors

interacted with one another, as well as how they behaved individually. The study design

in given in Table 1.

Table 1. Study design for discussed research project.

GROUP NUMBER	MICROGRID	WIREBRUSH CLEANING	NANOTUBES
1 (Grid+WB+NT)	❖	❖	❖
2 (Grid+WB)	❖	❖	
3 (Grid+NT)	❖		❖
4 (Grid)	❖		

❖ Indicates presence of treatment

Results

Microgrid Characterization

Figure 6 shows a representative top down SEM view of a portion of a laser deposited microgrid. Figure 7 shows a top down view of an entire titanium sample, after laser deposition, imaged on an optical microscope. Pore size was measured to be 600 μm ± 20 μm.
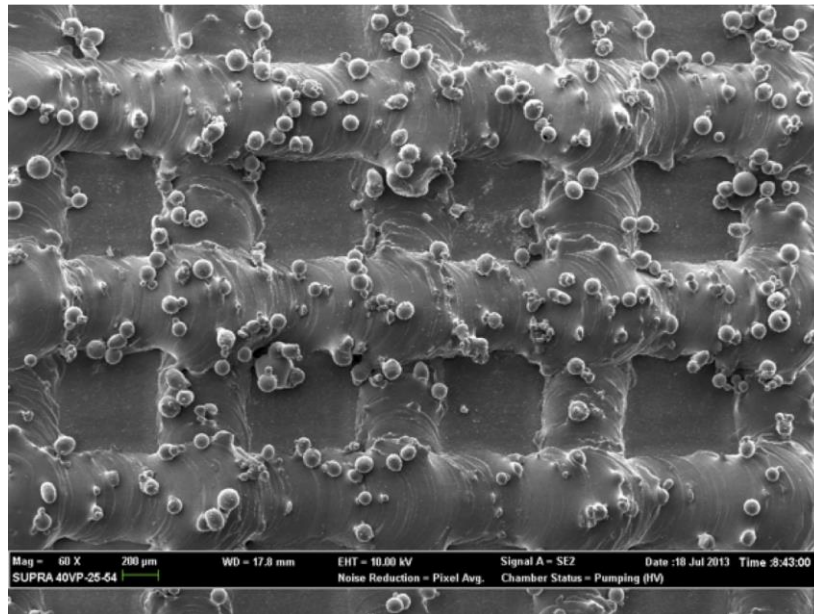
Figure 6. Top-down SEM image of laser deposition microgrid.
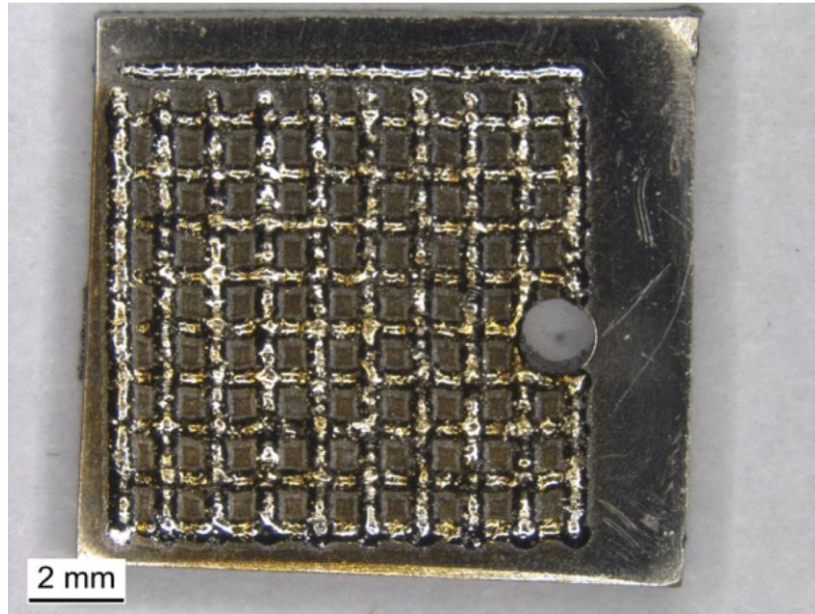
Figure 7. Top-down image of laser deposited microgrid titanium substrate.

Wirebrush Treatment

Figures 8 and 9 show SEM images of the same titanium substrate, before and after wirebrush treatment, respectively.
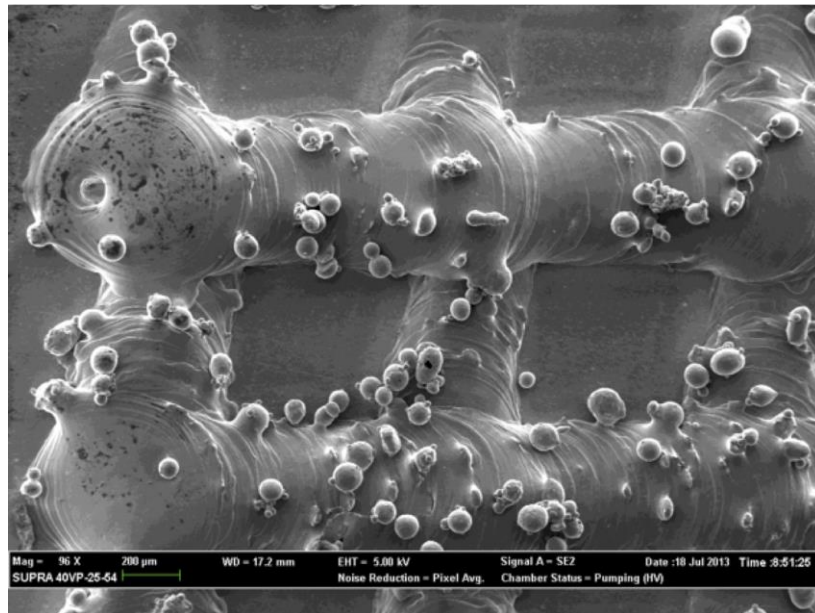

Figure 8. Top-down SEM image of substrate before wirebrush treatment.
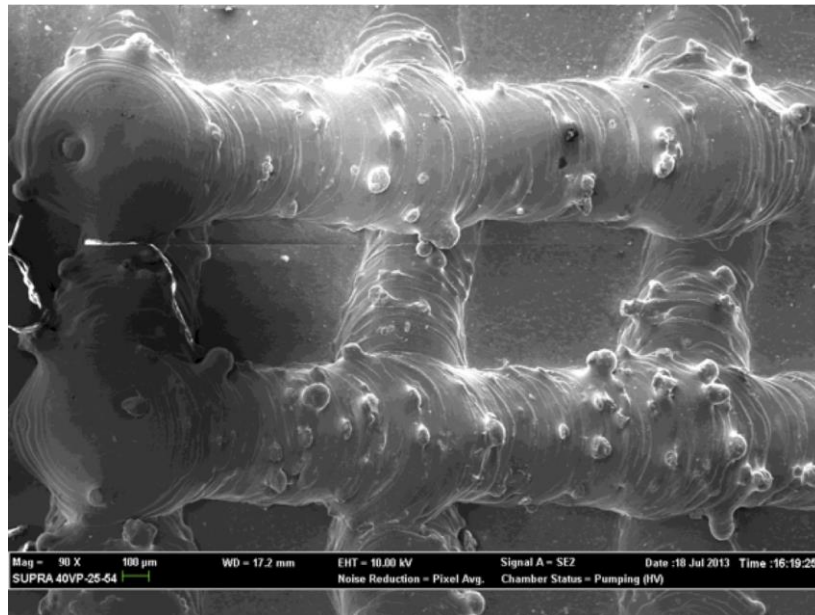
Figure 9. Top-down SEM image of substrate after wirebrush treatment.

From inspection of Figures 8 and 9, wirebrush treatment dramatically decreased the amount of unmelted laser deposition particles remaining on the surface after LD.

Nanotubes Characterization

Figure 10 shows a side view of the nanotubes. Using side-view pictures of the nanotubes and ImageJ image analysis software, nanotube length was measured to be 714 nm ± 34 nm.
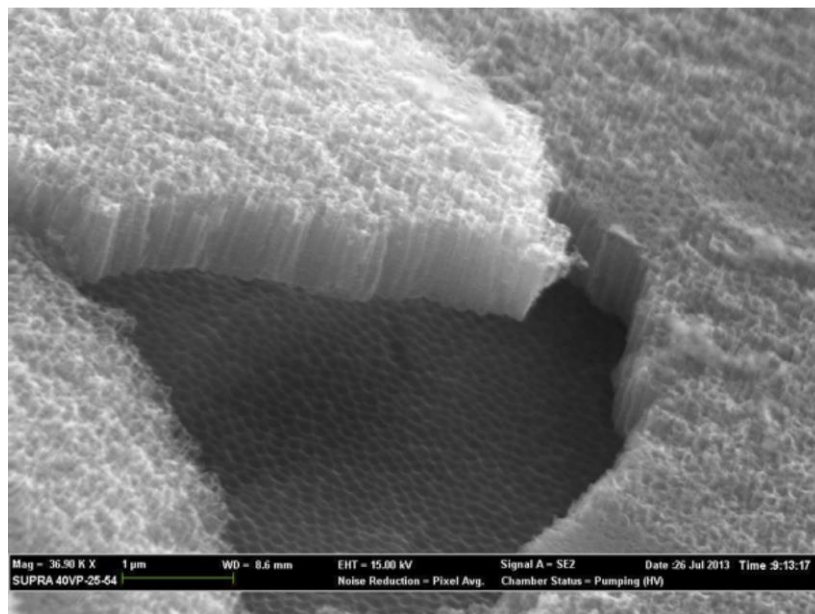

Figure 10. SEM side view of nanotubes

Figure 11 shows a top-down view of the nanotubes, imaged to show the structure of the tubes. Using top down images and ImageJ image analysis, nanotubes diameter was measured to be 88 nm ± 6 nm.
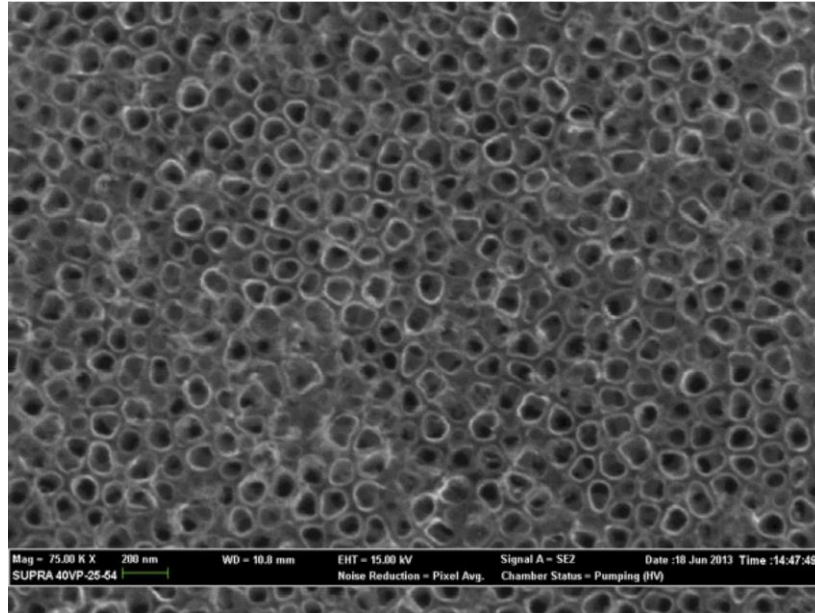

Figure 11. SEM top-down view of TiO$_2$ nanotubes.

Contact Angles

The sessile drop method was used to determine contact angle. Representative images of sample contact angles are presented in Figure 12 and the average contact angles for each group are presented in Table 2. As is evident, surfaces with nanotubes showed significantly lower contact angles when compared to surfaces with no nanotubes. Additionally, the sample that underwent only wirebrush treatment had a contact angle approximately 17 degrees less than the sample that received no treatment, proving wirebrush treatment also reduced contact angle.
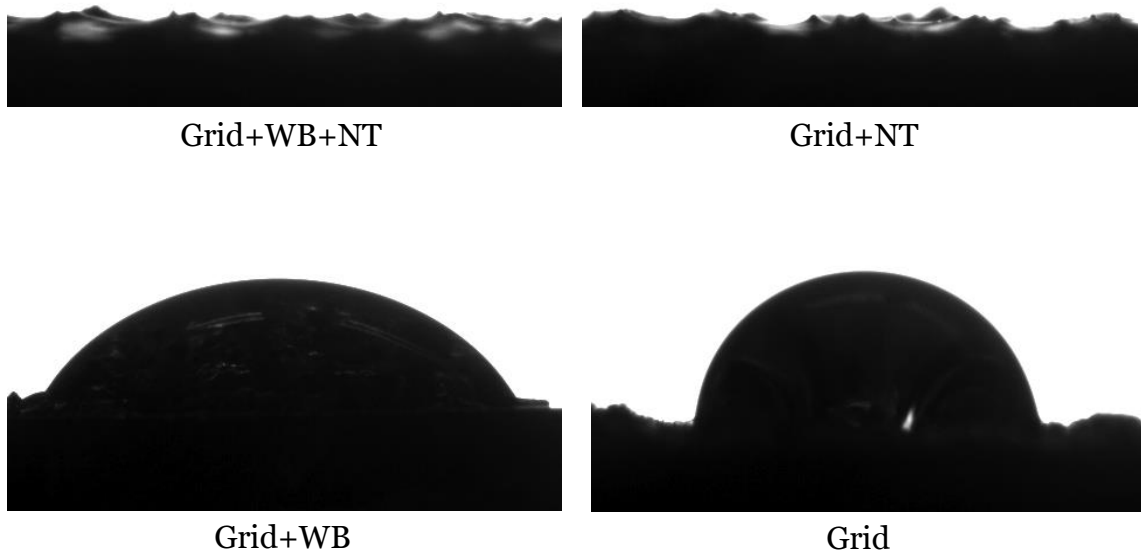
Grid+WB+NT   Grid+NT

Grid+WB   Grid

Figure 12. Representative sessile drop images used to measure contact angle.

Table 2. Calculations of average contact angles for study.

Group	Average Contact Angle (degrees)
Grid+WB+NT	N/A
Grid+NT	N/A
Grid+WB	57.2 ± 1.4
Grid	74.5 ± 4.9

Cell Morphology

Previous work performed by Sauter showed cell morphologies amongst the groups did not yield many differences. Because of this, only one separate sample was used to check the morphology of the cells. Figures 13 and 14 show high and low

magnification images of the cells after incubation for four hours, respectively. After four hours, the cells showed signs of cell adhesion and cell spreading. It was also evident that the cells were attaching in greater quantities in the pores, rather than on the microgrid itself.
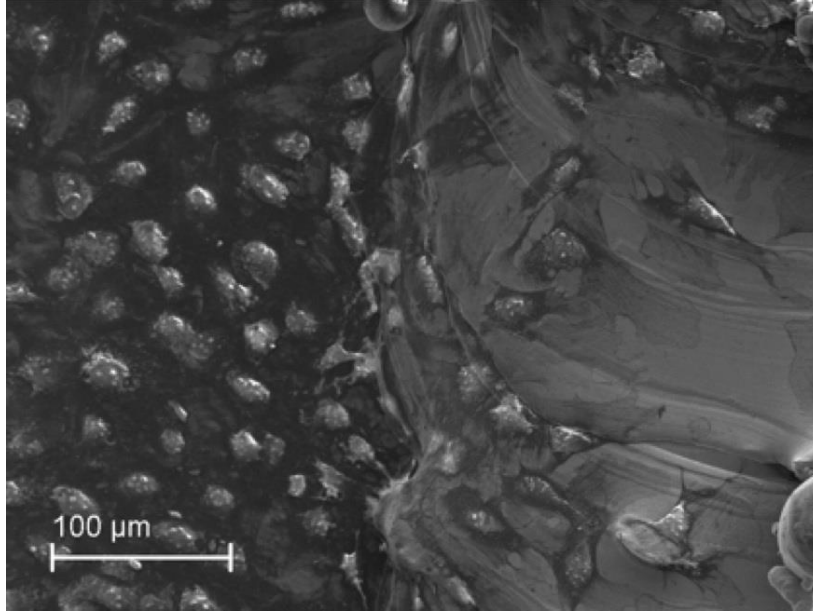

Figure 13. SEM image of fixed mouse pre-osteoblasts on sample. Substrate (pore) is on left, laser deposited grid is on right.
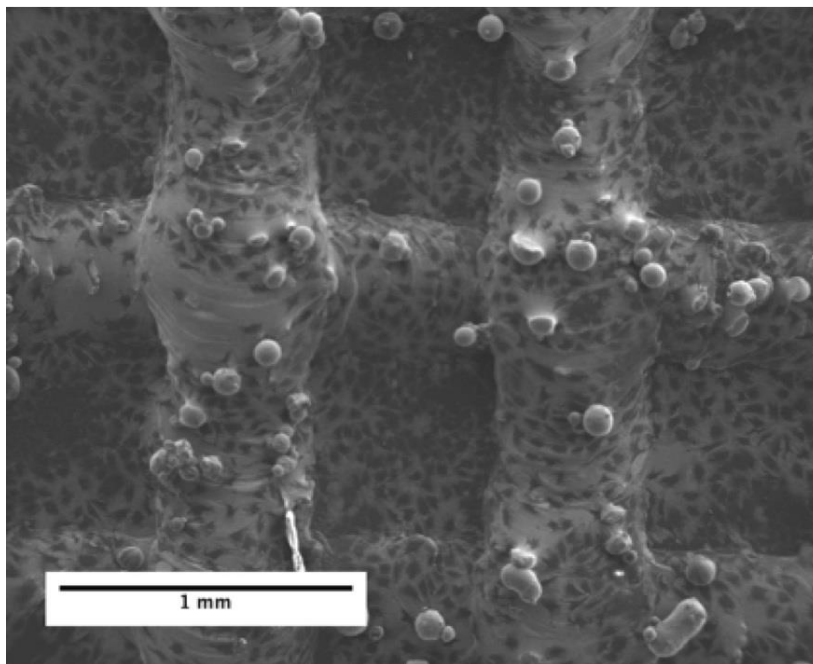

Figure 14. SEM image of fixed mouse pre-osteoblasts on sample.

Cell Viability

Figure 15 shows the fluorescent microscope images of mouse osteoblasts on the different experimental groups. Qualitatively, groups that had nanotubes on the surface stained brighter for live cells than groups with no nanotubes. Additionally, wirebrush treated groups stained more positively for cells than groups without wirebrush treatment.
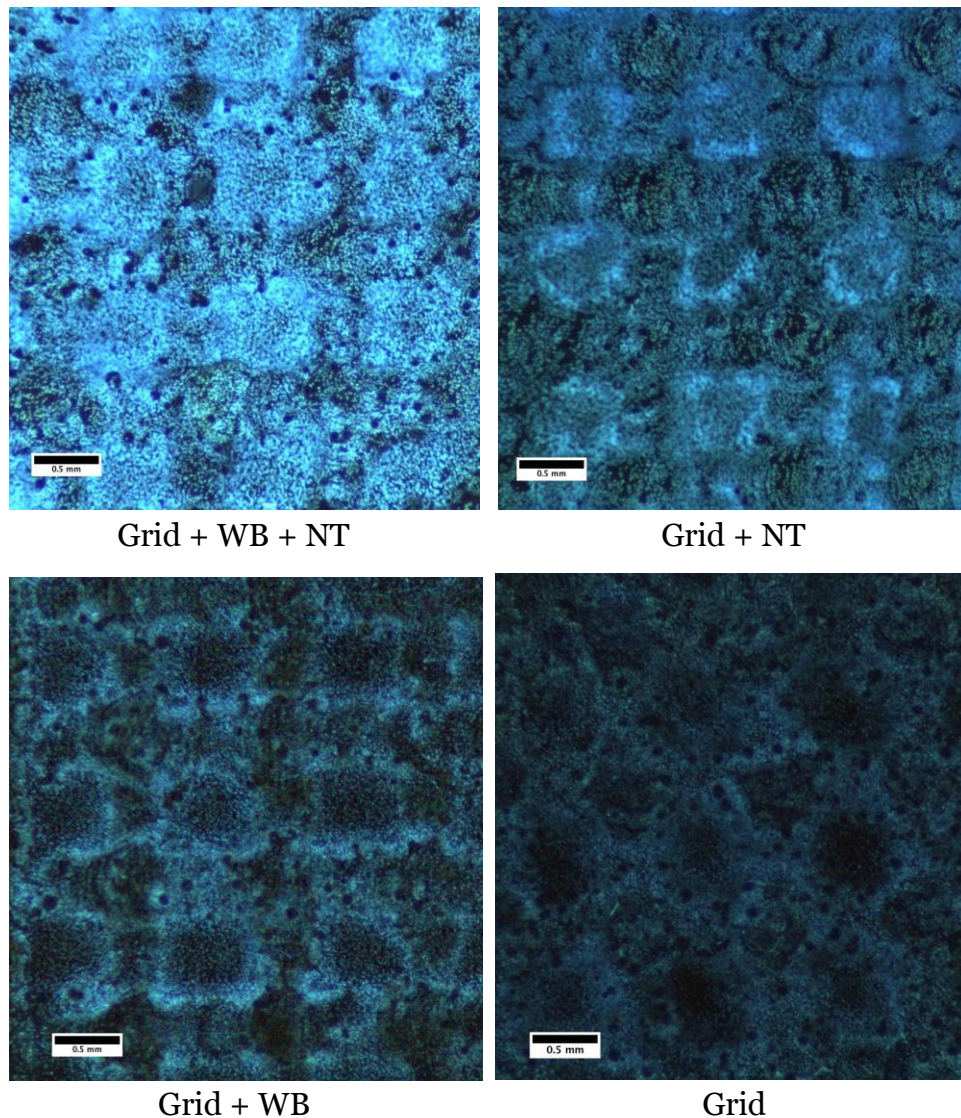

Grid + WB + NT   Grid + NT

Grid + WB   Grid

Figure 15. Representative images of fluorescently stained cell nuclei after a four-day incubation period.

Quantitatively, the same results followed; the group with dramatically greater cell adhesion compared to all other groups was the group that underwent wirebrush treatment and had nanotubes. Figure 16 shows Sauter's previous cell density data quantified in the same manner, for reference. Additionally, Table 3 shows the fluorescence intensities of all groups in this study.
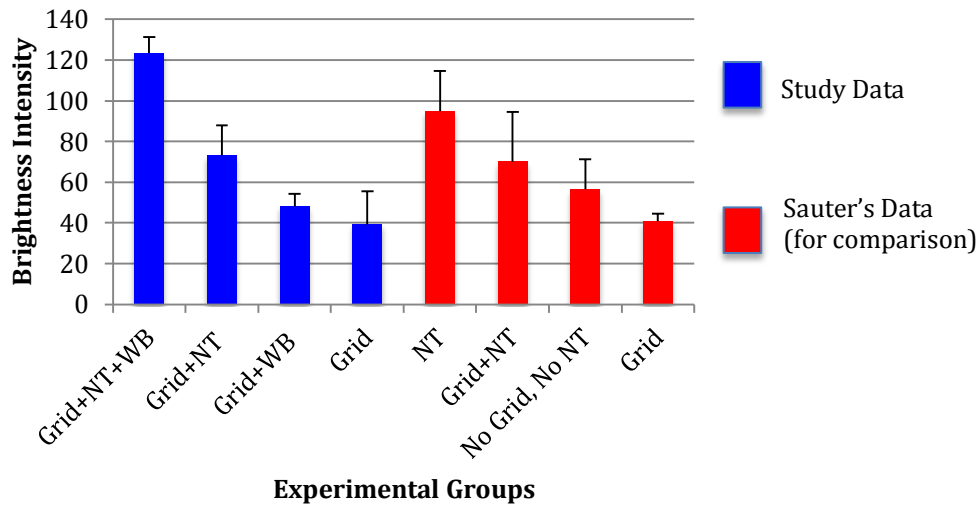

Figure 16. Bar graph of average fluorescence intensities (on a scale ranging from 0-255, 255 representing total brightness and 0 representing total darkness). Note: Error bars represent one standard deviation.

Table 3. Raw values of fluorescence intensities with one standard deviation.

Group	Fluorescence Intensity (unitless)
Grid+WB+NT	123.6 ± 7.80
Grid+NT	73.1 ± 15.0
Grid+WB	48.1 ± 6.20
Grid	39.2 ± 16.2

As a reference, Sauter's group with the highest cell density had an average fluorescence intensity of 94.8 ± 19.7, so it was obvious that minimizing the unmelted laser deposition particles was beneficial.

From inspection of Figure 16, three conclusions can be made. First, this study showed similar cell viability results when comparing matching treatments from Sauter's study. For example, Grid samples showed the poorest performance for both studies with an average brightness of 39 ± 16 and 40 ± 8 for this study and the reference study, respectively. This conclusion is critical as it permits further comparison between this study and the reference study. Furthermore, Graph 1 shows that wire brush treatment may result in a minor increase in cell viability for unanodized grid surfaces. For anodized surfaces, however, cell viability was dramatically improved over anodized grid surfaces without wirebrush treatment. In addition, wirebrush treated grid surfaces with nanotubes showed the highest intensity of all treatments in this study and the reference study.

Discussion

This study examined the hypothesis that the hierarchical surface coating for titanium implants, void of any aluminum contamination as well as unmelted laser deposition particles would enhance the properties of the substrates, and as a result, biological performance. This hypothesis was strongly supported. By shrinking the size of the grid, aluminum contamination was avoided. Anodized surfaces and surfaces that underwent wirebrush treatment cleaning showed lower contact angles to unanodized surfaces and surfaces that were not cleaned after laser deposition, respectively. Lower contact angles indicate a more hydrophilic surface. Hydrophilic surfaces foster better

protein adsorption, and as a result, better cell adhesion and osteoblast function [10]. Because of this, it was exciting to find the surfaces with nanotubes and the surfaces cleaned with a wirebrush showed lower contact angles.

Cell viability results for the study were also promising. As hypothesized, the groups with both components of the hierarchical coating showed better cell adhesion, compared to groups that only had the micro-scale portion of the coating. Additionally, as hypothesized, wirebrush treatment successfully removed unmelted laser deposition titanium particles, therefore removing a possible obstruction to the cells attaching. Consequently, surfaces that underwent wirebrush treatment showed greater cell attachment compared to samples that did not. Significantly, cell viability for surface treatments that incorporated TiO_2 nanotubes and properly cleaned (wirebrush) micro-scale grid structures was dramatically greater than that for TiO_2 nanotubes or micro-scale surface treatments alone. The reason for the dramatic increase in cell viability on hierarchical surface treatments is not yet clear, however, the conclusion does speak to the positive impact of a hierarchical surface treatment and future study is needed.

Conclusion

This study evaluated the processing, microstructure characterization and in vitro biological performance of hierarchical surface treatments on Ti substrates. The results showed that the Ti surface with nanotubes as well as wirebrush treatment had dramatically better biological response. Additionally, surfaces with the hierarchical coating showed improved properties when compared to surfaces with only the microgrid.

Lastly, wirebrush treatment was also shown to improve the biological response of the substrates.

This study provides justification for further investigation of hierarchical surface modifications, consisting of micro-scale and nano-scale surface features, for improvement of early osseointegration behavior of titanium implants. The microgrid pore sizes of this study were approximately 600 μm; however, further research should be done to reduce the size of the microgrid pore size, as the optimal pore size has been found to be between 100 μm-200 μm. Optimization of the hierarchical coating, especially the microstructure may possibly lead to greater cell adhesion.

With improved osseointegration, the mechanical fixation between the medical implant and bone will be stronger, leading to longer-lasting, more successful implants.

References

1. American Academy of Orthopaedic Surgeons. (2011). OrthoInfo. *Total Hip Replacement*. Retrieved June 27, 2013, from http://orthoinfo.aaos.org/topic.cfm?topic=A00377.

2. American Academy of Orthopaedic Surgeons. (2011). OrthoInfo. *Total Knee Replacement*. Retrieved June 27, 2013, from http://orthoinfo.aaos.org/topic.cfm?topic=A00389.

3. Arthritis Foundation. (2008). Osteoarthritis Fact Sheet. *Disease Center, Osteoarthritis.* Retrieved June 24, 2013, from http://www.arthritis.org/files/images/newsroom/media-kits/Osteoarthritis_fact_sheet.pdf.

4. Bitton, R. (2009). The economic burden of osteoarthritis. *Am J Manag Care, 15*(8 Suppl), S230-235.

5. Buckland-Wright, C. (2004). Subchondral bone changes in hand and knee osteoarthritis detected by radiography. *Osteoarthritis Cartilage, 12 Suppl A*, S10-19.

6. Kohal, R. J., Bachle, M., Att, W., Chaar, S., Altmann, B., Renz, A., & Butz, F. (2013). Osteoblast and bone tissue response to surface modified zirconia and titanium implant materials. *Dent Mater, 29*(7), 763-776. doi: 10.1016/j.dental.2013.04.003

7. Li, L. H., Kong, Y. M., Kim, H. W., Kim, Y. W., Kim, H. E., Heo, S. J., & Koak, J. Y. (2004). Improved biological performance of Ti implants due to surface modification by micro-arc oxidation. *Biomaterials, 25*(14), 2867-2875. doi: 10.1016/j.biomaterials.2003.09.048

8. Liu X. Y., Chu P. K., Ding C. X. 2004. Surface modification of titanium, titanium alloys, and related materials for biomedical applications. Mater. Sci. Eng. Rep. 47, 49–121.

9. Merashly, M., & Uthman, I. (2012). Management of knee osteoarthritis: an evidence-based review of treatment options. *J Med Liban, 60*(4), 237-242.

10. Messina, G. M., Satriano, C., & Marletta, G. (2009). A multitechnique study of preferential protein adsorption on hydrophobic and hydrophilic plasma-modified polymer surfaces. *Colloids Surf B Biointerfaces, 70*(1), 76-83. doi: 10.1016/j.colsurfb.2008.12.013

11. Mueller, C. K., Solcher, P., Peisker, A., Mtsariashvili, M., Schlegel, K. A., Hildebrand, G., . . . Schultze-Mosgau, S. (2013). Analysis of the influence of the

macro- and microstructure of dental zirconium implants on osseointegration: a minipig study. *Oral Surg Oral Med Oral Pathol Oral Radiol, 116*(1), e1-8. doi: 10.1016/j.oooo.2011.10.041

12. Murphy, L., & Helmick, C. G. (2012). The impact of osteoarthritis in the United States: a population-health perspective: A population-based review of the fourth most common cause of hospitalization in U.S. adults. *Orthop Nurs, 31*(2), 85-91. doi: 10.1097/NOR.0b013e31824fcd42

13. Sauter, E. (2013). *Processing, Microstructure Characterization and Biological Performance of Hierarchical Surface Coatings for Titanium Implants.* Unpublished master's thesis, South Dakota School of Mines and Technology, Rapid City, South Dakota.

14. Sista, S., Nouri, A., Li, Y., Wen, C., Hodgson, P. D., & Pande, G. (2013). Cell biological responses of osteoblasts on anodized nanotubular surface of a titanium-zirconium alloy. *J Biomed Mater Res A*. doi: 10.1002/jbm.a.34638

15. Song, W., Yu, X., Markel, D. C., Shi, T., & Ren, W. (2013). Coaxial PCL/PVA electrospun nanofibers: osseointegration enhancer and controlled drug release device. *Biofabrication, 5*(3), 035006. doi: 10.1088/1758-5082/5/3/035006

Acknowledgments